

Crucial Parameters and Optimization of High-Speed Bearingless Drives

Hubert Mitterhofer and Siegfried Silber

Linz Center of Mechatronics GmbH
Altenbergerstrasse, 69 - 4040 Linz, Austria
hubert.mitterhofer@lcm.at, siegfried.silber@lcm.at

Abstract — Bearingless drives integrate the functionality of magnetic bearings and an electric machine into a single device. While this integration allows very compact drives offering all advantages of magnetic levitation, the design process becomes significantly more complex. This work deals with the numerous topological and geometric design decisions which need to be taken for such a bearingless drive. Additionally, the definition of suitable optimization targets for the electromagnetic simulation process is outlined. The proposed guidelines generate a complex relationship of different dependencies which is then fed into the *MagOpt* optimizer for the design of a high speed bearingless disk drive, which allows verifying the optimization results through measurement results from two prototype drives.

Index Terms — Bearingless drive, force and torque evaluation, *MagOpt*, optimization.

I. INTRODUCTION

Magnetic bearings dispose of several characteristics which have allowed them to conquer certain fields of applications requiring, e.g., high-purity, long lifetime, or high rotational speeds. By integrating magnetic bearings and electric drives in a bearingless drive, the mechanical dimensions become more compact while the complexity in design, optimization, and control increases.

The design process of a high-speed bearingless drive demands several topological decisions. Section 0 presents the most stringent choices and discusses their respective influence on the drive performance. Section 0 first deals with the remaining geometric parameters and selects the actual optimization parameters. Before the optimization, not only the parameters but also the targets need to be defined. Other than in the design of conventional electrical machines, literature presents no widely used performance parameters since both, the torque and the bearing performance including their cross-coupling and their angle dependency are relevant. Therefore, this work proposes suitable optimization targets, characterizing different aspects of the performance of a bearingless disk drive. Their use as target values allows applying optimization tools, in this case, the general purpose

optimizer *MagOpt*.

Eventually, the optimization results for two certain designs are given in section 0. The comparison with the measurements at two actually constructed prototypes shows the benefits of the optimization.

II. TOPOLOGICAL DECISIONS

A. Machine topology

Bearingless drives have been constructed using different machine topologies, from classic permanent magnet synchronous machines (PMSMs) to induction machines or reluctance based types. A good overview about the early developments is given in [1]. However, for achieving full levitation with a mechanically compact design, the PMSM topology with a permanent magnet rotor is the preferable solution. Additionally, high energy density and good efficiency, even for small drives, speak in favor of this motor topology. Therefore, as for most recent developments, the PMSM topology is chosen for the targeted high-speed drive.

B. Rotor

A disk-shaped rotor can be chosen over an elongated rotor because of its passive stability in axial and tilt directions [2]. Supplemented with the active stabilization in radial direction by the bearingless unit, stable levitation can be achieved with one bearing point.

For high rotational speeds, an inner rotor with two-pole magnetization has been used in the drives presented in [3], [4] or [5]. The inner rotor with its smaller diameter is subject to lower centrifugal forces. The low pole number results in the highest mechanical frequency for a given electrical frequency. However, the two-pole diametrical magnetization also adds anisotropic stiffness characteristic to the drive. Viewed in the stationary coordinate system, the effect can, e.g., be written for the destabilizing radial reluctance force as:

$$F_{r,rel} = \begin{bmatrix} \bar{c}_r(1 + \hat{c}_r \cos(2\Omega t)) & \bar{c}_r \hat{c}_r \sin(2\Omega t) \\ \bar{c}_r \hat{c}_r \sin(2\Omega t) & \bar{c}_r(1 - \hat{c}_r \cos(2\Omega t)) \end{bmatrix} \begin{bmatrix} \Delta x \\ \Delta y \end{bmatrix}, \quad (1)$$

with Δx and Δy , being the stator-bound radial deflections. Ω gives the angular frequency of rotation and \bar{c}_r and \hat{c}_r

stand for the mean stiffness value and its variation ratio, respectively. An equal formulation is possible for the stabilizing tilt reluctance torque. More details on this matter can be found in [6].

Despite this complexity increase for the system, the effect on a rotor is negligible when we can assume operation at high rotational speeds since Equation (1) clearly shows that the principal frequency of the anisotropic force on a deflected rotor is twice as high as the frequency of rotation and, therefore, quickly surpasses the radial rigid body mode, given as:

$$\omega_r = \sqrt{\frac{\bar{c}_r}{m_{rotor}}}, \quad (2)$$

with m_{rotor} standing for the rotor mass.

C. Stator core

One of the main topological decisions concerns the used stator material. While laminated electrical steel with low hysteresis losses is surely preferable for low speed applications, high frequencies of the rotating magnetic field provoke high eddy current losses which may call for the use of soft magnetic composite (SMC) material. These sintered materials feature very low electric conductivity and thus, low eddy current losses which scale according to:

$$p_{Fe,ed} \sim f^2, B^2, \quad (3)$$

where f and B denote the principal frequency of the magnetic field and the flux density, respectively. Due to the hysteresis losses which dominate in SMC materials, scaling according to:

$$p_{Fe,h} \sim f, B^2, \quad (4)$$

there is a break-even point for a certain field frequency above which SMC is beneficial. In literature (e.g., in [7]), this point is typically found to be between 1 kHz and 2 kHz, depending on the quality of the compared SMC and laminated steel materials, which makes the use of SMC interesting in high-speed drives. Due to the potential advantage concerning the core loss and the additional simplicity in prototyping (the SMC can be milled from a block form), the SMC material *Somaloy 700 5P* is selected for the current analysis.

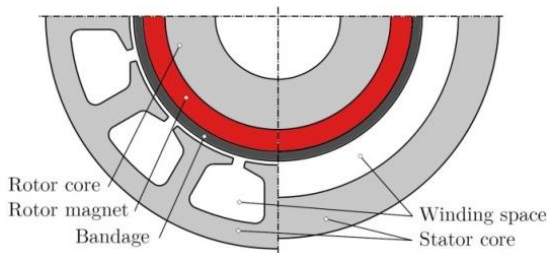


Fig. 1. Slotted (left) and slotless (right) stator topology.

A second principal decision for the stator design

concerns the question if a slotted or a slotless core shall be applied (cf. Fig. 1). While the former provides small magnetic air gaps and, thus, high air gap flux density, the latter offers low stator losses due to the sinusoidal flux density distribution, the absence of higher slot harmonics, and the wider air gap. For very high speed machines, it has been shown in literature, e.g., in [4] or [8] and [9], that the slotless core is the better choice.

D. Winding system

The proposed slotless stator form directly triggers the decision between air gap winding or toroid winding. Both are depicted in Fig. 2. While electromagnetically equal, the toroid winding has the more compact mechanical form with reduced copper volume when a flat rotor shape is used [10]. Additionally, it offers simple prototype manufacturing and good cooling properties. Manufacturing in an automated process may be more complex than for the air gap winding but overall, the toroid winding seems advantageous.

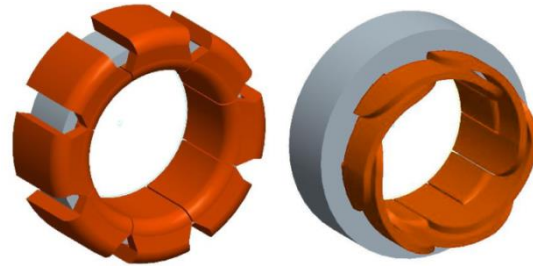


Fig. 2. Toroid winding (left) and air gap winding (right).

Concerning the winding connection topology, it is possible to differ between the following configurations.

1) Separated windings

When multiple sets of windings are used, i.e., one for torque and another one for bearing force creation, the term *separate winding system* is applied. In this case, the necessary currents and voltages for the motor and bearing function are calculated, applied, and controlled separately. This poses a very intuitive approach to the problem of parallel torque and force creation which is frequently used and well documented in numerous publications, e.g., [11], [12].

2) Combined windings

For additional mechanical simplification, the reduction to a single back iron core with one single set of windings is possible. The current components for torque and forces now have to be superposed before being applied to the drive. In this so-called *combined winding system*, the simplification of the mechanical setup increases the control complexity. Many studies have dealt with this winding type, e.g., [13], [14], or [5].

3) Dual-purpose no-voltage windings

A third winding topology has appeared recently ([15], [16], [18]), partly mixing the properties of separated and the combined windings. It provides combined windings with different coil terminals for torque and force current connections by tapping the respective coils. This is termed *parallel motor winding* or *bridge winding* and can, more generally be found in literature as *dual-purpose no-voltage (DPNV) windings*. However, this topology can increase the amount of necessary power switches and current sensors significantly as shown in [16]. Additionally, a full description of the multiple DPNV connection possibilities would go beyond the scope of this work but can be found in the cited publications.

The authors of [17] have compared separated and combined winding systems for a disk shaped bearingless radial pump. Another work [18] discusses the differences between two DPNV winding types and eventually compares them to a separated winding system. All these considerations have come to the conclusion that the correct winding choice is highly dependent on the available power electronics. One of the most stringent differences, however, is the sensitivity to the rotor-field induced back-EMF which must be analyzed in order to allow a topology decision.

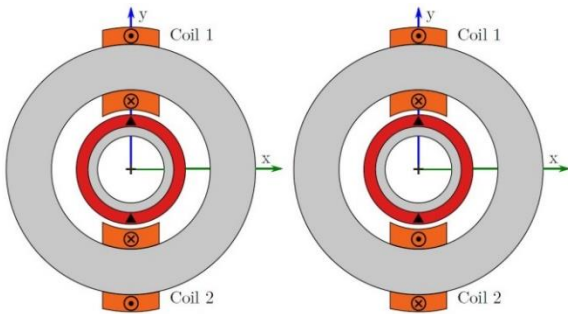


Fig. 3. Separated winding example for bearing forces (left) or torque creation (right) with a two-pole rotor.

The separated winding example in Fig. 3 shows two configurations of coils, each wound around a slotless stator core in a toroid winding manner. They can be connected in order to produce bearing forces (identical winding sense) and torque (opposing winding sense), respectively. Coil 1 and Coil 2 have an identical number of winding turns and, thus, identical values for resistance $R = R_1 = R_2$, inductance $L = L_1 = L_2$, and linked rotor flux amplitude $\hat{\psi} = \hat{\psi}_1 = \hat{\psi}_2$. Due to the winding sense, it becomes clear that the back-EMF V_{BEMF} in the two coils adds up for the torque winding while it cancels out in the force winding setup. Figure 4 shows this relationship in an equivalent circuit. When the voltage drops in L_1 and L_2 cancel out in the torque winding due to the opposing winding sense, the voltage at the clamps

of a connected full bridge inverter is:

$$V_{bridge,T} = i_T 2R + 2\hat{\psi} \cos(\omega t) \omega, \quad (5)$$

where i_T gives the torque current and ω specifies the electrical angular frequency. With a DC-link voltage of V_{DC} , the maximum rotational frequency is limited to:

$$\omega_{max} = \frac{V_{DC} - i_T 2R}{2\hat{\psi}}. \quad (6)$$

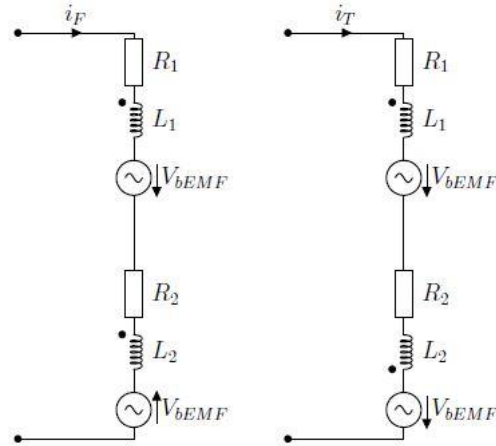


Fig. 4. Equivalent circuit for force (left) and torque creation (right) in the separated winding shown in Fig. .

In a combined winding scheme, each of the coils needs to be controlled individually which results in the corresponding circuit diagram shown in Fig. 5.

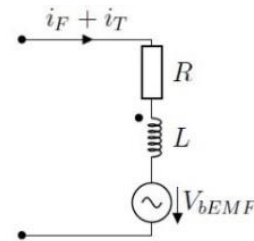


Fig. 5. Equivalent circuit for a combined winding system.

In analogy to the separated winding described above, the clamp voltage at a full bridge is expressed as:

$$V_{bridge} = (i_F + i_T)R + L \frac{d(i_F + i_T)}{dt} + \hat{\psi} \cos(\omega t) \omega, \quad (7)$$

since neither the inductive voltage drop nor the back-EMF cancels out. This limits the maximum rotational frequency to:

$$\omega_{max} = \frac{V_{DC} - (i_F + i_T)R - L \frac{d(i_F + i_T)}{dt}}{\hat{\psi}}. \quad (8)$$

As the back-EMF component is relevant for both, torque and force creation, a voltage reserve needs to be respected in order to guarantee that even at maximum speed, the system can react sufficiently to a radial

disturbance by injecting the necessary force currents.

At a first glance, the combined winding topology seems disadvantageous due to the independence of the force creation from V_{BEMF} . However, this apparent flaw can be resolved by respecting the said voltage reserve. Also, the combined winding always uses the entire conductor cross section which increases efficiency. Lower part count and maximum mechanical compactness add to the advantages of the combined winding which is why it is chosen here.

At the beginning of Section 0, the toroid winding form is presented as an alternative to the air gap winding which in turn was deducted from the winding in a slotted motor. Therefore, each phase shown in the left image in Fig. 6 consists of two coil halves which, together, are electrically equivalent to the air gap winding. This is called *double coil* arrangement. It is, however, also possible, to use only one half per phase (right part in Fig. 6) forming a *single coil* arrangement. Both forms are used for the optimization process below.

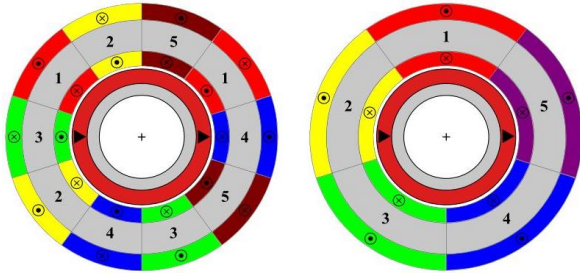


Fig. 6. Exemplary double coil (left) or single coil (right) arrangement for a drive with eight phases.

III. OPTIMIZATION

With a chosen stator (slotless SMC core), a certain winding structure (toroid) with a selected connection (combined winding), the most influential remaining topological choices are the coil number per phase (single or double coil) and the number of phases. The different features of the resulting options have been discussed in [5], leaving the single coil scenarios with 6 or 8 phases as the most beneficial ones. However, for the sake of comparability with preceding studies, only the 5-phase double coil (5pd) and the promising 6-phase single coil (6ps) and 8-phase single coil (8ps) arrangements are selected for optimization.

A. Geometric parameters

Different geometric parameters characterize the drive. In the present case, the rotor diameter d_{ro} and the rotor magnet height h_{PM} are set to a fixed value (cf. Table 1), making the further radial parameters, the rotor back iron (yoke) height h_Y , the height of the rotor bandage h_B , the air gap width δ , the height of the coils

h_{coil} , and the stator height h_{Fe} relevant for the design. Furthermore, the axial stator length l_{Fe} and the phase number m are varied in order to find the best choice.

The parameters h_B and δ are determined by the mechanical safety demands, the necessary touchdown bearing dimensions, and the manufacturing tolerances and will not be used as optimization parameters. The remaining optimization parameters are listed in Table 2.

Table 1: Optimization data – fixed parameters

Fixed Parameter	Value
d_{ro}	30 mm
h_{PM}	4.5 mm
δ	1.5 mm
Coil topology	5pd, 6ps, 8ps

Table 2: Optimization data – variables and targets

Variable Parameter	Range	Target	Limit Value
h_Y	2.5 – 3 mm	c_z	$> 2 \frac{N}{mm}$
h_{coil}	2 – 3.5 mm	c_τ	$> 0.8 \frac{Nm}{rad}$
h_{Fe}	9 – 13 mm	$k_{startup}$	< 2
l_{Fe}	10 – 14 mm	\bar{T}_z	$> 45 mNm$

B. Optimization targets

The passive stiffness coefficients and the active bearing performance are the most important properties besides the torque capacity. Unfortunately, high passive stiffness calls for small magnetic air gaps while active forces and torque require the exact opposite in order to provide a large copper cross section for the stator coils. This conflict can be solved by defining the necessary conditions for the drive in order to function properly and leave the remaining parameters to optimization. In [5], multiple criteria have been defined of which are briefly explained below.

1) Radial force

The active radial force F_r must overcome the passive radial reluctance force, defined in Equation (1). This allows setting a necessary criterion:

$$F_r(\varphi, -\vartheta) > F_{r,rel}(\vartheta - \varphi)\delta \quad \forall \varphi, \vartheta \in [0, 2\pi], \quad (9)$$

for guaranteeing the rotor lift-off for every possible initial rotor deflection angle ϑ , determining the necessary force direction as $-\vartheta$, and every rotor orientation angle φ . The achievable radial force is maximized for the nominal current density J_{max} while zero drive motor torque T_z is produced:

$$F_{r,max}(\varphi, -\vartheta) = \max F_r(\varphi, -\vartheta) |_{J_{1..m} \leq J_{max}, T_z = 0}. \quad (10)$$

For a practical and meaningful value, the radial reluctance force can be substituted by the radial stiffness value and then be put into relation with the maximized

radial force. For a worst-case startup current coefficient, this ratio needs to be maximized, yielding:

$$k_{startup} = \max_{\forall \varphi, \vartheta \in [0, 2\pi]} \frac{\bar{c}_r (1 + \hat{c}_r \cos(2(\vartheta - \varphi))) \delta}{F_{r,max}(\varphi, -\vartheta)}, \quad (11)$$

which, multiplied with J_{max} , must not exceed the short-time tolerable overload current density $J_{startup}$.

2) Axial stiffness

For guaranteeing a limited axial deflection $\delta_{z,max}$ of the rotor due to gravitational acceleration g , the axial stiffness constant must satisfy:

$$c_z > \frac{m_{rotor} g}{\delta_{z,max}}. \quad (12)$$

3) Torque and tilt stiffness

When the necessary criteria in Sections 1) and 2) are met, the drive torque T_z and the tilt stiffness c_τ can be maximized as remaining optimization targets. As the drive torque value also needs to be evaluated under the maximum current density constraint and the independency from the radial forces, a similar criterion as for the forces can be written for the mean torque as:

$$\bar{T}_z = \frac{1}{2\pi} \int_0^{2\pi} \max(T_z(\varphi) |_{J_{1..m} \leq J_{max}, F_x=F_y=0}) d\varphi. \quad (13)$$

C. Optimization setup

Before optimization, the simulation setup is verified by comparing simulation and measurement for two available prototypes. These have different geometric parameters and dispose of a 5pd and a 6ps winding, respectively. All target parameters obtained in simulation except for the tilt stiffness have been measured and the values given in Table 3 show good agreement with an acceptable error of $\leq 10\%$.

Table 3: Comparison of simulated and measured data

	5pd Design		6ps Design	
	<i>Sim.</i>	<i>Meas.</i>	<i>Sim.</i>	<i>Meas.</i>
c_z in $\frac{N}{mm}$	2.31	2.21	1.782	1.84
c_τ in $\frac{Nm}{rad}$	0.749	n.a.	0.565	n.a.
$k_{startup}$	2.19	2.29	2.605	2.81
\bar{T}_z in <i>mNm</i>	24.0	22.92	38.97	37.39

For the actual optimization, *MagOpt*, developed at LCM GmbH, was used. *MagOpt* provides an interface to several commercial and open-source programs such as CAD and finite element tools via the respective APIs. After configuring a simulation chain with starting

parameters and result targets, the built-in genetic optimizer is used to automatically run the simulations. An initial generation of parameter sets is created, sent to the parametric model in a 3D FE solver, in this case, *Ansoft Maxwell*, and the results are obtained from the simulation output. After processing the results, the next generation of data sets is created, sent to the solver, etc. As the numerical simulation itself can be considered a standard procedure for the design of electric drives and magnetic bearings, the automated optimization is the key feature for this parameter-heavy design process. Within a matter of days, several thousand parameter sets are numerically evaluated, converging to the specified targets, forming the resulting Pareto fronts.

IV. ANALYSIS AND CONCLUSION

A. Analysis of the result

The automated optimization process is stopped when the Pareto front shown in Fig. 7 converges and no longer produces new individuals in the graph. The top left and the bottom right graphs which display the two passive stiffnesses and the two active torque or force targets, respectively, are not useful for finding the optimal individuals. In these two images, both displayed targets benefit from and are weakened by the same geometrical changes. The remaining four graphs compare targets which show opposed reactions to a geometry variation. It is these graphs that the optimum needs to be selected from. It quickly becomes clear that the 5-phase, 6-phase, and 8-phase designs do not differ in the passive stiffness targets as these results do not depend on the winding characteristics. The most prominent difference appears in the torque capacity where the 6ps and 8ps designs dominate. This is the only feature where the topology choice is significantly more important than the geometric choice.

After filtering the solutions according to the target limits given in Table 2, the ones marked with red circles in Fig. 7 remain. For each phase number, one individual is selected and shown in Table 4. While all three meet the targets, the 6ps and 8ps designs are clearly favorable.

Table 4: Selected individuals

Parameter	5pd	6ps	8ps	Target	5pd	6ps	8ps
h_V in <i>mm</i>	2.91	2.94	2.96	c_z in $\frac{N}{mm}$	2.03	2.14	2.17
h_{coil} in <i>mm</i>	3.3	3.21	3.27	c_τ in $\frac{Nm}{rad}$	0.84	0.82	0.85
h_{Fe} in <i>mm</i>	9.63	9.82	10.51	$k_{startup}$	1.63	1.68	1.73
l_{Fe} in <i>mm</i>	13.4	12.7	13.95	\bar{T}_z in <i>mNm</i>	47.6	69.2	76.4

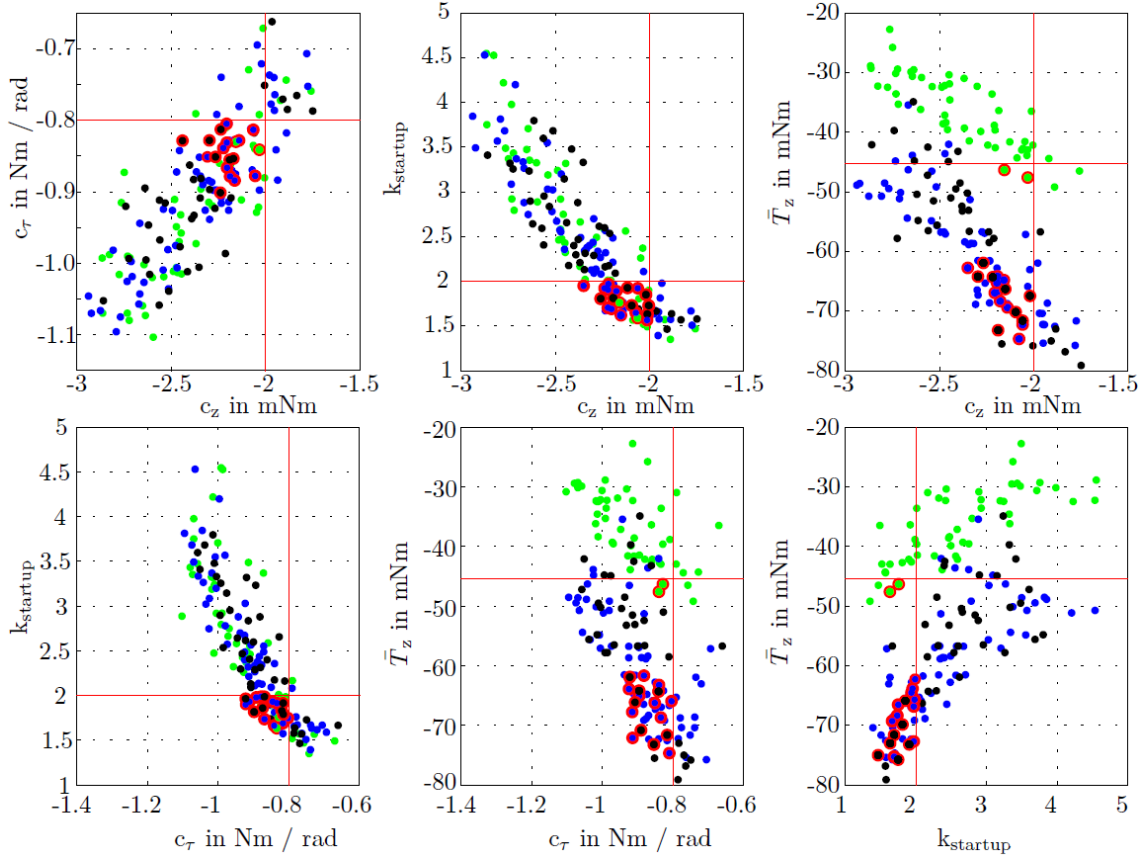


Fig. 7. Optimization output: Pareto fronts with 5pd variants (green) and 6ps variants (blue). Individuals marked red fulfill all targets indicated as red lines.

V. CONCLUSIONS

The design of bearingless drives is a complex undertaking which is expressed by the plurality of topological decisions to take and the numerous geometric parameters influencing the drive performance. Several interesting conclusions can be drawn from the design process.

Characteristic requirements such as high speed, high torque or high efficiency need to be respected in every design step and cannot be left to optimization alone. This is especially true for the selection of the winding topology and the phase number which heavily influence the necessary power electronics circuit.

However, even if certain topological decisions are taken in advance, a multi-criteria optimization based on numerical electromagnetic simulation is necessary due to the large number of influential parameters. Also, the definition of optimization targets is significantly more complex than with a conventional electric machine and their number is higher since active and passive magnetic forces need to be considered.

Even if MagOpt does not restrict the number of variable parameters or targets, a large number of either one will make the optimization process lengthy and the

results hard to interpret. Therefore, it is important to stick to realistic parameter ranges and necessary targets.

ACKNOWLEDGEMENT

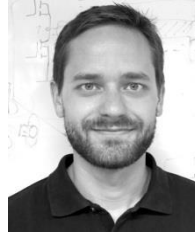
This work was conducted within the COMET-K2 program of the Linz Center of Mechatronics (LCM), and was funded by the Austrian Federal Government and the Federal State of Upper Austria. The authors thank all involved partners for their support.

REFERENCES

- [1] A. Salazar, A. Chiba, and T. Fukao, "A review of developments in bearingless motors," *Proc. 7th Int. Symp. on Magnetic Bearings*, 2000.
- [2] R. Schoeb and N. Barletta, "Principle and application of a bearingless slice motor," *Proc. 5th Int. Symp. on Magnetic Bearings*, 1996.
- [3] H. Mitterhofer, W. Gruber, and W. Amrhein, "On the high speed capacity of bearingless drives," *IEEE Trans. on Ind. Electronics*, vol. 61, no. 6, pp. 3119-3126, 2014.
- [4] D. Steinert, T. Nussbaumer, and J. W. Kolar, "Slotless bearingless disk drive for high-speed and high-purity applications," *IEEE Trans. on Ind.*

- Electronics*, vol. 61, 2014.
- [5] H. Mitterhofer, B. Mrak, and W. Gruber, "Comparison of high-speed bearingless drive topologies with combined windings," *IEEE Trans. on Ind. Applications*, vol. 51, no. 3, pp. 2116-2122, 2015.
 - [6] H. Grabner, H. Bremer, W. Amrhein, and S. Silber, "Radial vibration analysis of bearingless slice motors," *Proc. 9th Int. Symp. on Magnetic Bearings*, 2004.
 - [7] A. Schoppa, P. Delarbre, E. Holzmann, and M. Sigl, "Magnetic properties of soft magnetic powder composites at higher frequencies in comparison with electrical steels," *Proc. 3rd Int. Electric Drives Production Conference*, 2013.
 - [8] A. Chebak, P. Viarouge, and J. Cros, "Analytical computation of the full load magnetic losses in the soft magnetic composite stator of high-speed slotless permanent magnet machines," *IEEE Trans. on Magnetics*, vol. 45, pp. 952-955, 2009.
 - [9] T. Baumgartner, A. Looser, C. Zwysig, and J. W. Kolar, "Novel high-speed, Lorentz-type, slotless self-bearing motor," *Proc. Energy Conversion Congress and Exposition*, 2010.
 - [10] H. Mitterhofer, H. Grabner, and W. Amrhein, "Comparison of two and four pole rotors for a high speed bearingless drive," *Proc. 13th Int. Symp. on Magnetic Bearings*, 2012.
 - [11] A. Chiba, D. T. Power, and M. A. Rahman, "Characteristics of a bearingless induction motor," *IEEE Trans. on Magnetics*, 1991.
 - [12] P. Karutz, T. Nussbaumer, W. Gruber, and J. W. Kolar, "The bearingless 2-level motor," *Proc. 7th Int. Conf. on Power Electronics and Drive Systems*, 2007.
 - [13] W. Gruber, T. Nussbaumer, H. Grabner, and W. Amrhein, "Wide air gap and large-scale bearingless segment motor with six stator elements," *IEEE Trans. on Magnetics*, 2010.
 - [14] T. Reichert, T. Nussbaumer, and J. W. Kolar, "Bearingless 300-W PMSM for bioreactor mixing," *IEEE Trans. on Ind. Electronics*, 2012.
 - [15] A. Chiba, S. Horima, and H. Sugimoto, "A principle and test result of a novel bearingless motor with motor parallel winding structure," *Proc. Energy Conversion Congress and Exposition*, 2013.
 - [16] E. Severson, S. Gandikota, and N. Mohan, "Practical Implementation of dual purpose no voltage drives for bearingless motors," *Proc. IEEE Applied Power Electronics Conference and Exposition*, 2015.
 - [17] K. Raggl, T. Nussbaumer, and J. W. Kolar, "Comparison of winding concepts for bearingless pumps," *Proc. Int. Conf. on Power Electronics*, 2007.
 - [18] E. Severson, R. Nilssen, T. Undeland, and N. Mohan, "Dual-purpose no-voltage winding design for the bearingless AC homopolar and consequent

pole motors," *IEEE Trans. on Ind. Applications*, vol. 51, no. 4, pp. 2884-2895, 2015.



Hubert Mitterhofer studied Mechatronics at Johannes Kepler University (JKU), Austria and Université de Pierre et Marie Curie, France and received his diploma in 2008 and his Ph.D. degree in 2017. Since 2013, he is working as a Researcher at the Linz Center of Mechatronics GmbH (LCM), dealing with electrical drive development, bearingless high speed drives and magnetic bearings. Mitterhofer is involved in the development of MagOpt and is maintaining the web portal magneticbearings.org. His personal technical interests also cover agriculture technology and renewable energies.



Siegfried Silber studied Electrical Engineering at the University of Technology Graz and obtained his Dr.Techn. degree from JKU Linz, Austria, in 1995 and 2000, respectively. He was with the Institute for Electrical Drives and Power Electronics at the JKU from 1995 to 2014 and joined LCM in 2014 where he is Technical Area Manager for Electrical Drives. His research interests include electrical drives, power electronics, magnetic bearings and bearingless motors. Silber is leading the development of the mechatronic component optimizer MagOpt and the open source tool X2C for model-based development and code generation of real-time control algorithms for microprocessor units.